Measurements of Moisture Transport in Wood-Based Materials under Isothermal and Nonisothermal Conditions

Samuel V. Glass, PhD
Associate Member ASHRAE

ABSTRACT

Building envelopes in various climates are exposed to a broad range of temperature and moisture conditions. Moisture transfer across the building envelope by diffusion in the hygroscopic range usually involves a thermal gradient as well as a water vapor pressure gradient. While many studies using common building materials have explored the dependence of water vapor permeability on relative humidity (RH), very few measurements have been made to characterize the effect of temperature under isothermal conditions or the effect of a thermal gradient. These effects may be of special importance in wood-based building materials. In our experiments, water vapor permeance is measured by sealing a material between two chambers that are independently controlled; temperature, RH, and the rate of mass transfer are measured on both sides of the specimen. Results are reported for 11-mm-thick plywood at room temperature and compared with other isothermal permeability data from the literature. Three experiments with conditions of nearly constant water vapor pressure in the presence of a thermal gradient show small moisture flows from high RH to low RH (from the cold side to the warm side) that might have been caused by water vapor pressure gradients within the experimental error. These result are discussed in the context of similar experiments in the literature.

INTRODUCTION

The importance of moisture management in buildings has gained much attention in recent years. The consequences of uncontrolled moisture flows and moisture accumulation can be severe: mold growth, decay, corrosion, staining, and even structural failure. While much progress has been made in understanding the physics of moisture in buildings and using computer modeling as a basis for moisture-control engineering (Hens 1996, Karagiozis 2001), there still remain many unanswered questions.

In reality, building envelopes are exposed to a broad range of temperature and moisture conditions. Moisture transfer across the building envelope by diffusion usually involves a thermal gradient as well as a vapor pressure gradient. Hence there is a need for accurate measurements of material characteristics spanning a broad range of temperature and humidity conditions (Bomberg 2006). Although much research has been directed towards the dependence of water vapor permeability on relative humidity for many materials (see, for example, Kumaran 1996, 2002), there are currently no definitive conclusions about the magnitude or significance of thermally-driven moisture transport. Indeed, accurately characterizing the effect of a thermal gradient on moisture transport is an experimental challenge.

Previous Experiments

An obvious location for large thermal gradients in building envelopes is insulating materials. Thermally-driven moisture transport has been shown to make a significant contribution to the total moisture flow through glass fiber and cellulose insulation (Kumaran 1987, 1988, 1989; Peuhkuri 2003), as well as rock wool, flax, and perlite insulation (Peuhkuri 2003). More complex behavior has been observed in polyurethane and polyisocyanurate foam insulation (Schwartz et al. 1989), while conflicting results have been found in extruded polystyrene insulation (Dahl et al. 1996, Galbraith et

S.V. Glass *is a research physical scientist at the USDA Forest Products Laboratory, Madison, WI.*

al. 1998a). Investigations of dense porous materials have suggested that a thermal gradient can induce significant moisture transport in gypsum board (Galbraith et al. 1998a, Krus 1996) and sandstone (Krus 1996).

Wood and wood-based materials present a combination of characteristics that may result in nonisothermal moisture transport playing a significant role: a moderate thermal conductivity, a high degree of moisture sorption, and a strong dependence of moisture permeability on relative humidity. A large body of work has been aimed at understanding nonisothermal moisture transport in wood (see Avramidis 1994 and references cited therein; Krus 1994; Segerholm 2002, 2003). Nonisothermal experiments have also been conducted with wood-based products including "chipboard" (Krus 1992, 1996) and oriented strand board (Dahl et al. 1996, Thomas 1999).

In addition to the effect of a thermal gradient, a number of experiments have explored the effect of varying the temperature (under isothermal conditions). Several experiments covering a variety of building materials have shown no significant temperature effect (Burch et al. 1992, Mukhopadhyaya et al. 2005, Tveit 1966, Valovirta and Vinha 2004). However, Chang and Hutcheon (1956) observed an increase in permeability with temperature for asphalt-saturated felt and building paper. Schwartz et al. (1989) likewise showed that the permeabilities of polyurethane and polyisocyanurate foam insulations increase significantly with temperature. Galbraith et al. (2000) found the same trend for plywood and medium density fiberboard but no significant temperature effect for gypsum board or phenolic foam insulation. Clearly, more work is needed to clarify where thermal gradients and varying temperature levels might have a significant effect in real building envelopes.

Moisture Transport Equations

Various driving potentials may be selected to model moisture flow. These include temperature, relative humidity, water vapor pressure, water vapor density, liquid capillary pressure, suction pressure, moisture content, and chemical potential (Claesson 1993, Hens 1996). In general, there may be three independent state variables; however, when the air pressure is constant (which is nearly always the case), there are two independent variables. Commonly used potentials include temperature and water vapor pressure (Galbraith et al. 1997) or temperature and relative humidity (Künzel 1995).

Moisture transport under nonisothermal conditions can be modeled by an equation of the form

$$J_m = -\mu \nabla p_v - D_T \nabla T \,, \tag{1}$$

where

J_m = moisture flux in both vapor and liquid phases (i.e., mass of H_2O transmitted through unit area in unit time, $kg \cdot m^{-2} \cdot s^{-1}$);

μ = moisture permeability, $kg \cdot m^{-1} \cdot s^{-1} \cdot Pa^{-1}$;

p_v = water vapor pressure, Pa;

D_T = coefficient for thermally driven moisture flow, $kg \cdot m^{-1} \cdot s^{-1} \cdot K^{-1}$; and

T = temperature, K.

For hygroscopic materials such as wood, the moisture permeability increases rapidly with increasing relative humidity φ. This dependence can be described with a function known as the differential permeability $\mu(\varphi)$ (Chang and Hutcheon 1956).

In a given isothermal steady-state moisture transport experiment, the average permeability corresponding to the boundary conditions on each side of the material is measured. A vapor pressure gradient is established across the specimen of thickness Δx by maintaining the environment on one side at p_1 and on the other side at p_2. The average permeability $\bar{\mu}$ is calculated as

$$\bar{\mu} = \frac{-J_m \Delta x}{p_2 - p_1} \,. \tag{2}$$

The measured average permeability and differential permeability function are related (under isothermal conditions) by

$$\bar{\mu} = \frac{1}{p_2 - p_1} \int_{p_1}^{p_2} \mu \, dp_v = \frac{1}{\varphi_2 - \varphi_1} \int_{\varphi_1}^{\varphi_2} \mu \, d\varphi \,. \tag{3}$$

This relationship is depicted graphically by Chang and Hutcheon (1956) and McLean et al. (1990). The permeance M ($kg \, m^{-2} \, s^{-1} \, Pa^{-1}$) may also be reported; it is calculated as

$$M = \frac{-J_m}{p_2 - p_1} = \frac{\bar{\mu}}{\Delta x} \,. \tag{4}$$

Experimental Approaches

There are several ways to select boundary conditions for steady-state moisture transport experiments as shown in Figure 1 (Peuhkuri 2003):

1. Constant T: the p_v and φ gradients must be in the same direction;
2. Constant p_v: the T and φ gradients must be in opposite directions;
3. Constant φ: the T and p_v gradients must be in the same direction;
4. The T and p_v gradients may be in the same direction and opposite the φ gradient;
5. The p_v and φ gradients may be in the same direction and opposite the T gradient; and
6. The $T, p_v,$ and φ gradients may all be in the same direction.

It should be noted that $T, p_v,$ and φ are not independent, as discussed above; they are related by

$$p_v = \varphi \cdot p_{sat}(T) \tag{5}$$
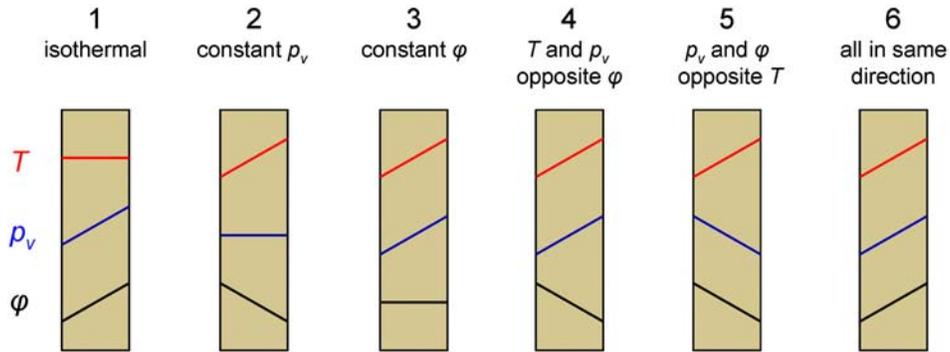
Figure 1 *Illustration of possible boundary conditions in steady-state moisture transport experiments (after Peuhkuri [2003]).*
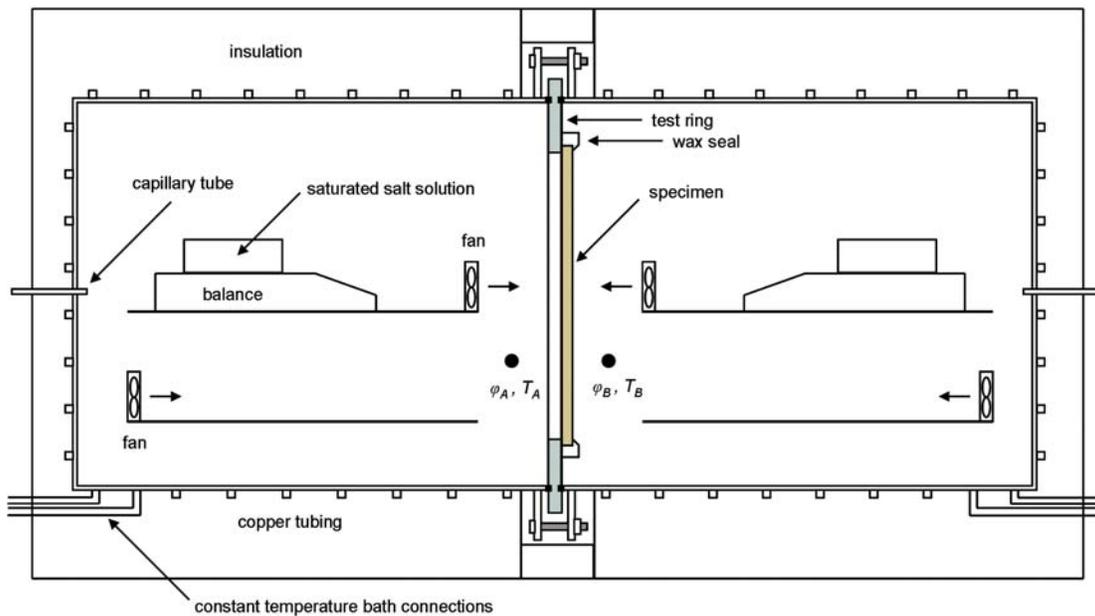
Figure 2 *Cross-sectional schematic of the experimental apparatus. The two chambers are identical. The temperature/humidity probes are represented by solid circles.*

where $p_{sat}(T)$ is the water vapor saturation pressure (Pa) at temperature T (K). Other combinations of driving potentials discussed above may be selected, giving rise to analogous types of boundary conditions.

The objective of this study was to characterize moisture transport in exterior-grade plywood under boundary conditions of the first two types shown in Figure 1.

EXPERIMENTAL METHODOLOGY

Materials

Measurements have been carried out with a specimen of circular cross-section cut from a 1.2 by 2.4 m board of exterior-grade (CDX) plywood composed of four plies of southern yellow pine. The diameter of the specimen is 311 ± 1.5 mm; its thickness is 11.0 ± 0.3 mm (nominally 15/32-in.); and its dry density is 530 ± 10 kg m^{-3}. Prior to any moisture transport experiments, the specimen was preconditioned for two months at 23 ± 1°C and 50 ± 2% RH.

Apparatus

The experimental apparatus is depicted in Figure 2 and has been described previously (Douglas 1991; Douglas et al. 1992, 1993; Dahl 1993; Dahl et al. 1996). In brief, the specimen is sealed between two stainless steel chambers in which temperature and relative humidity are independently controlled. Temperature, RH, and the rate of moisture transfer are measured

on both sides of the specimen. The apparatus resides in a laboratory maintained at 23 ± 1°C and 50 ± 2% RH.

Isothermal and nonisothermal experiments can be carried out at an anticipated temperature range of 0°C to 50°C. Temperature control is achieved by circulating a fluid (water for the experiments reported here) from a constant temperature bath through a network of copper tubing surrounding the chambers. Each chamber has its own tubing network and bath and is insulated for temperature stability, which has been measured to be within ±0.05°C for temperatures between 20°C and 27°C.

The chambers are approximately cylindrical, with a diameter of ~400 mm and a depth of ~450 mm. The specimen is sealed with microcrystalline wax to a test ring constructed from a glass woven epoxy composite, which has a low thermal conductivity, low moisture permeability, and low moisture capacity. A circular groove is machined on each side of the test ring for seating a gasket. When the test ring is positioned between the two chambers, these gaskets mate with the chambers' lips. The assembly is fastened by six bolts mounted on aluminum flanges. An acrylic spacer on each bolt helps to support and position the test ring.

The relative humidity in each chamber is regulated by an aqueous saturated salt solution. Each solution is contained in an open dish (100 mm diameter, 50 mm high) placed on a precision balance with ±2 mg repeatability. The mass of the solution is recorded at regular time intervals to determine the moisture transfer rate for each chamber. The salt solutions give very stable relative humidities over extended periods (Greenspan 1977). The temperature and RH of the air near the specimen (within 20 mm) are measured by calibrated probes. Each probe consists of a platinum resistance thermometer and a capacitive thin film humidity sensor. In addition, four type-T thermocouples measure temperature in various locations in each chamber. In order to avoid stratification, the chamber air is mixed by a pair of DC axial fans. A capillary tube 1.6 mm in diameter by 1.2 m long connects each chamber to the surrounding environment so that there is no significant air pressure gradient across the specimen. The instrument power and signal wires are connected through two 12-pin feedthroughs at the back of each chamber. Measurements are recorded by a computer-based data acquisition system at regular time intervals—typically 1 or 2 minutes.

Procedures

Aqueous saturated salt solutions are prepared in glass dishes and placed on the balances in each chamber. The specimen and test ring are then positioned and fastened between the chambers, and data acquisition commences. The experiment is ended when a sufficient amount of time has passed at a steady-state condition—that is, where the temperature, relative humidity, and rate of moisture transfer in each chamber are deemed to be constant. In order to minimize the error in the measured moisture transfer rate, a change in mass of at least 500 mg is desirable under steady-state conditions. The time required to reach steady-state is typically between one and three weeks for 11-mm-thick plywood.

Table 1 lists the solutions and the measured relative humidity conditions for the isothermal set of measurements at $23.0 \pm 0.15°C$ ($p_{sat} = 2.81 \pm 0.02$ kPa). The theoretical values of relative humidity are calculated from Greenspan (1977). The boundary conditions for the nonisothermal experiments conducted at nearly constant water vapor pressure are shown in Table 2. These conditions were intended to match case 2 in Figure 1. During Experiment I, the mass transfer rate measured in the cold, high RH chamber (A) could not be used for comparison because water vapor condensed on the chamber walls. The resulting condensation, however, did not adversely affect the water vapor pressure; the standard deviation of the mean p_v (16 Pa) was still within the experimental uncertainty (±30 Pa due to uncertainty in measuring T and φ; see below). The water vapor pressures at steady-state were quite stable for Experiments II and III, with the standard deviation being less than 2 Pa. There was no condensation on the chamber walls in these experiments (a slightly lower RH was selected for the cold chamber). Prior to the second nonisothermal experiment, improvements were made to the apparatus in the attempt to minimize leakage. The gaskets were replaced,

Table 1.   Conditions for Isothermal Experiments

Experiment	Chamber	Solution	Theoretical φ	Measured φ	p_v, kPa
1	A	LiCl	0.11	0.12 ± 0.01	0.34 ± 0.03
	B	$MgCl_2$	0.33	0.32 ± 0.01	0.90 ± 0.03
2	A	K_2CO_3	0.43	0.45 ± 0.01	1.26 ± 0.03
	B	NaBr	0.58	0.58 ± 0.01	1.63 ± 0.03
3	A	K_2CO_3	0.43	0.46 ± 0.01	1.29 ± 0.03
	B	NaCl	0.75	0.72 ± 0.01	2.03 ± 0.03
4	A	NaBr	0.58	0.59 ± 0.01	1.67 ± 0.03
	B	KCl	0.85	0.81 ± 0.01	2.27 ± 0.03
5	A	NaBr	0.58	0.60 ± 0.01	1.70 ± 0.03
	B	KNO_3	0.94	0.87 ± 0.01	2.44 ± 0.04

Table 2. Conditions for Nonisothermal Experiments

Experiment	Chamber	Solution	T, °C	p_{sat}, kPa	Theoretical φ	Measured φ	p_v, kPa
I	A	KCl	20.5	2.41 ± 0.02	0.85	0.83 ± 0.01	1.999 ± 0.03
	B	NaBr	27.0	3.57 ± 0.03	0.57	0.56 ± 0.01	1.990 ± 0.03
II	A	NaCl	20.7	2.44 ± 0.02	0.75	0.75 ± 0.01	1.835 ± 0.03
	B	$Mg(NO_3)_2$	26.7	3.50 ± 0.03	0.52	0.52 ± 0.01	1.826 ± 0.03
III	A	NaCl	20.8	2.45 ± 0.02	0.75	0.75 ± 0.01	1.847 ± 0.03
	B	$Mg(NO_3)_2$	27.0	3.57 ± 0.03	0.52	0.52 ± 0.01	1.853 ± 0.03

Table 3. Estimates of Experimental Uncertainty

Measurement	Absolute Uncertainty	Relative Uncertainty
Specimen area A		$\pm 1\%$
Temperature T	± 0.15°C	
Water vapor saturation pressure $p_{sat}(T)$		$\pm 0.9\%$
Relative humidity $\varphi < 0.90$	± 0.01	
Relative humidity $\varphi \geq 0.90$	± 0.02	
Total moisture transfer rate $\dot{m}_{total}$		$\pm 0.5\%$
Moisture leakage rate m_{leak}	± 200 ng·s^{-1}	
Masked edge correction factor c_{edge}		$\pm 0.9\%$
Surface air layer resistance Z_a		$\pm 10\%$

and the grooves in the test ring were re-machined to ensure smooth surfaces for seating the gaskets. Polyethylene bags were sealed to the exterior ends of the capillary tubes to prevent moisture from escaping while still allowing the chambers to equalize in pressure with the laboratory. However, these measures did not eliminate moisture exchange between the chambers and the laboratory. Therefore leakage rates were determined with the chambers maintained under nearly the same conditions as in Experiments II and III.

Sources of Uncertainty

The uncertainty in the measured permeance M (ng·m^{-2}·s^{-1}·Pa^{-1}) depends on the cumulative uncertainty from several measurements. In addition to random errors in the measurement of temperature, relative humidity, the rate of moisture transfer, and the area of the specimen, there are three systematic errors inherent in the test method that need to be accounted for (Douglas 1991): (i) leakage of water vapor between the chambers and the ambient environment; (ii) two-dimensional diffusion within the edge of the specimen masked by the wax seal; and (iii) resistance to water vapor transfer due to the air layers at the specimen surfaces. A thorough discussion and analysis of experimental error is given in Appendix A. When the corrections for these systematic errors are incorporated, permeance is calculated as

$$M = \frac{1}{\dfrac{A \cdot p_{sat}(T) \cdot \Delta\varphi}{\dot{m} \cdot c_{edge}} - Z_a}, \tag{6}$$

where

A = exposed surface area of the specimen (m^2);

$p_{sat}(T)$ = water vapor saturation pressure (Pa) at temperature T (K);

$\Delta\varphi$ = $\varphi_A - \varphi_B$, the difference in relative humidity across the specimen (dimensionless);

$\dot{m}$ = $\dot{m}_{total} - \dot{m}_{leak}$, the rate of water vapor transmission through the specimen (ng·s^{-1}), being the total measured rate of moisture transfer minus the rate of leakage between the chamber and the laboratory;

c_{edge} = correction factor for diffusion within the edge of the specimen masked by the wax seal (dimensionless); and

Z_a = resistance to water vapor transfer due to the air layers at both surfaces of the specimen (m^2·s·Pa·ng^{-1}).

Table 3 summarizes the estimated uncertainties in the various measurements. Cumulative uncertainty depends on the test conditions, with $\Delta\varphi$ and $\dot{m}$ having the largest contributions. Isothermal permeance measurements typically have an error of ± 7–15%, while nonisothermal moisture flux measurements may have an error as low as $\pm 5\%$. However, as the magnitude of the flux diminishes, the uncertainty increases significantly.

Table 4. Moisture Permeance of 11-mm-Thick CDX Plywood at 23.0 ± 0.15°C

φ_A	φ_B	Permeance M	
		ng·m^{-2}·s^{-1}·Pa^{-1}	perm
0.12	0.32	68 ± 8	1.18 ± 0.14
0.45	0.58	108 ± 16	1.88 ± 0.28
0.46	0.72	134 ± 10	2.33 ± 0.17
0.59	0.81	209 ± 18	3.66 ± 0.31
0.60	0.87	255 ± 18	4.46 ± 0.32

Although the experimental method used in this study has several sources of uncertainty in common with the well-known cup method (see Bomberg 1989, Hansen and Bertelsen 1989, Hansen and Lund 1990, Hoffee 1989, Joy and Wilson 1965, and Toas 1989), it overcomes a number of limitations. First, it permits accurate measurements under a wide range of temperature and humidity conditions, both isothermal and nonisothermal. Second, the relative humidity is measured on both sides of the specimen rather than assumed to be the equilibrium RH for the saturated solution in a closed system. These may not necessarily be the same because of mass and heat flux: the solution may not be saturated at the air-solution interface, or the temperature of the solution may differ from that of the air due to net evaporation or condensation. Tables 1 and 2 list both the equilibrium and measured RH values; significant differences do occur when there is a large moisture flux. Third, the rate of mass transfer is measured on both sides of the specimen. In most instances, as steady-state is approached, the moisture transfer rates on each side converge, permitting a more accurate determination of when the moisture transfer rate actually becomes constant. Fourth, since the air within the chambers is mixed by fans, there is no correction for diffusive resistance of stagnant air, and the resistances of the air layers at the surfaces of the specimen can be measured. Fifth, the aqueous saturated salt solutions provide very stable RH values; oscillations—a common problem when using an environmental chamber—are minimized. Finally, the capillary tubes ensure that both chambers are at the same total pressure; there is no significant moisture transfer induced by an air pressure gradient.[1]

RESULTS AND DISCUSSION

Isothermal Experiments

Table 4 gives the moisture permeance values obtained from the isothermal experiments. These results are plotted in Figure 3 as permeability values.[2] The data are fitted with a

Figure 3 *Isothermal moisture permeability data with differential permeability curve given by $\mu(\varphi) = 0.75 + 7.59 \cdot \varphi^{4.61}$ (see text).*

differential permeability curve (see Introduction) using an equation of the form,

$$\mu(\varphi) = A + B \cdot \varphi^C, \qquad (7)$$

with the fitting parameters A, B, and C determined from a non-linear least-squares regression analysis. This functional form has been shown to provide a good description of the relationship between differential permeability and relative humidity for a wide range of building materials (Galbraith et al. 1998b). Further isothermal experiments will be carried out at higher RH conditions and at several different temperatures to characterize the material more fully.

Figure 4 compares the differential permeability function obtained from the data in this work with other curves from the literature. Table 5 gives the experimental conditions and information about the specimens. The curves all follow a trend of increasing permeability with increasing RH, but the values differ by as much as a factor of four or more. Different genera and species of wood may be expected to differ significantly in permeability: for example, spruce is more permeable than southern yellow pine by a factor of three at 10% RH and by a factor of two at 80% RH (Kumaran 2002). Differences in the number of plies, the type of adhesive, and the conditions during the manufacturing process may also contribute to the variations in permeability. However, a study of the water vapor permeability of several wood-based materials including a number of oriented strand boards, plywood products, wood fiberboards,

---

[1] Water vapor may pass between the chamber and the laboratory through the capillary tube by diffusion or by airflow induced by fluctuations in barometric pressure. This small rate of leakage is accounted for by measurements described in Appendix A.

[2] Strictly, permeability values apply only to homogeneous materials; plywood is clearly inhomogeneous. However, permeability values are commonly reported in the literature for inhomogeneous materials, and this practice is followed in order to compare measurements in this study with other measurements of plywood of different thicknesses in the literature.

Table 5. Comparison of Properties of Exterior Plywood Used in Room-Temperature Isothermal Permeability Experiments

Reference	T, °C	Thickness, mm	Dry Density, kg·m^{-3}	Composition
This work	23	11.0 ± 0.3	530 ± 10	4-ply southern yellow pine
McLean et al. (1990)	20	12	564	5-ply Malaysian morranti
Burch et al. (1992)	24	13	509	Not specified
Burch and Desjarlais (1995)	24	12.1	578	Not specified
Kumaran (2002)	23	12	470 ± 5	Douglas fir
Osanyintola et al. (2006)	23	9	445	Spruce
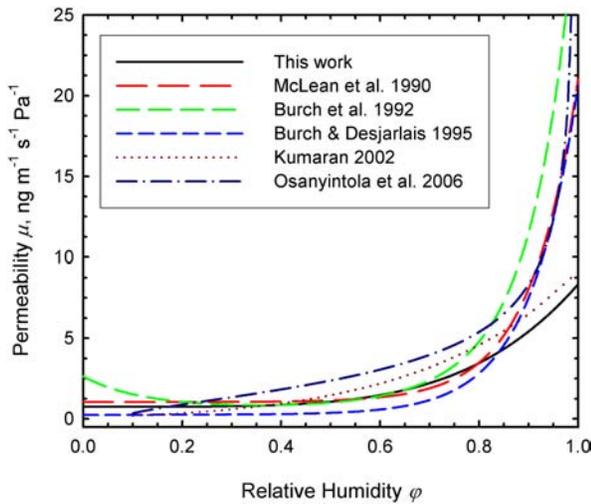
Figure 4 *Comparison of permeability functions for exterior-grade plywood at room temperature reported in the literature.*

and composite wood siding products found that the reproducibility across each type of material was within 15–30% (Kumaran et al. 2003). Differences due to the experimental technique should be relatively small: interlaboratory comparisons using standard test methods generally report reproducibilities of 10–20% (ASTM 2005, Galbraith et al. 1992, Kumaran 1998), although larger deviations have been reported (ASTM 2005, Hansen and Bertelsen 1989, Toas 1989).

Nonisothermal Experiments

The first nonisothermal experiment with nearly constant water vapor pressure across the specimen resulted in a moisture flux of $(8.0 \pm 2.7) \times 10^{-9}$ kg·m^{-2}·s^{-1} in the direction from high RH to low RH (cold to warm). Several factors contributed to the large uncertainty in the flux. In the warm, low RH chamber (B), the moisture flow through the specimen was nearly the same magnitude as the leakage of moisture from the chamber to the laboratory, resulting in a measured net rate of moisture transfer close to zero (see Appendix A for an analysis of experimental error). The mass transfer rate measured in the cold,

high RH chamber (A) could not be used for comparison because water vapor condensed on the chamber walls.

The subsequent nonisothermal experiments were conducted in order to reduce the uncertainties due to condensation and leakage. As there was no condensation on the chamber walls in these experiments, the moisture transfer rates measured in both chambers were averaged. The results are given in Table 6.

It can be shown that the moisture flux in all three experiments might have been caused by a possible water vapor pressure gradient that was within the experimental uncertainty. If p_v is assumed to be the only driving potential, the Δp_v necessary to induce the moisture fluxes for Experiments I, II, and III are 38 Pa, 28 Pa, and 5 Pa, respectively (see calculations in Appendix B). The experimental error in each measurement of p_v is ± 30 Pa, so the error in Δp_v is ± 40 Pa (square root of the sum of the squares, to one significant figure). On the other hand, if the experimental error is ignored, there is an apparent trend. In Experiments I and II, the moisture flux is clearly nonzero and in the direction from higher p_v to lower p_v. In Experiment III, the conditions were modified slightly from those of II in order to obtain a moisture flux as close to zero as possible. In this case, the Δp_v is smaller and in the opposite direction. If it is assumed that the moisture flux is driven by p_v, then the error in the measurement of Δp_v may be smaller than ± 40 Pa. However, when experimental uncertainties are properly considered, the data in this work are not sufficient to justify any conclusions regarding which gradient (T, φ, p_v, or some combination) is driving the observed moisture flux.

Thomas (1999) carried out nonisothermal measurements with 6.4-mm-thick oriented strand board (OSB). The experiments were designed to examine several driving potentials including water vapor pressure, water vapor concentration, moisture content, chemical potential, and activated moisture content. Boundary conditions were selected to determine whether moisture would flow when the driving potentials were the same on both sides of the specimen. Three experiments were conducted with conditions of constant water vapor pressure (case 2 in Figure 1). In all three cases the relative humidity was in the range 25–45%, and a moisture flux between 3.3 and 5.5×10^{-9} kg·m^{-2}·s^{-1} was measured in the direction from low RH to high RH (warm to cold). These small fluxes, similar in magnitude to those measured in this work, may also have been

Table 6. Moisture Flux through 11 mm Thick CDX Plywood under Nonisothermal Conditions

Experiment	φ_A	φ_B	$(p_{vA} - p_{vB})$, Pa	Moisture Flux (A → B), kg·m^{-2}·s^{-1}
I	0.83	0.56	9 (± 40)	$(8.0 \pm 2.7) \times 10^{-9}$
II	0.75	0.52	9 (± 40)	$(4.4 \pm 1.3) \times 10^{-9}$
III	0.75	0.52	−6 (± 40)	$(0.8 \pm 2.9) \times 10^{-9}$

caused by a Δp_v within the experimental uncertainty (see calculations in Appendix B). In fact, of all the driving potentials investigated, constant water vapor pressure came closest to zero moisture flux.

Dahl et al. (1996) also reported two experiments with 6.4-mm-thick OSB at nearly constant p_v. First, in the low RH regime (33% to 54%), the direction of moisture flow was from high RH to low RH (cold to warm). On the basis of the reported temperature and RH values, the difference in water vapor pressure was ~80 Pa, and the moisture flow was from high p_v to low p_v. The moisture flux of 1.22×10^{-8} kg m^{-2} s^{-1} could be explained by a p_v difference of 120 Pa, which falls within the error bars of the measured Δp_v (see calculations in Appendix B). Second, in the high RH regime (58% to 93%), moisture flowed from the side of low p_v (low RH, high T) to that of high p_v (high RH, low T), though Δp_v was only ~60 Pa. The experiment was carried out twice, and the observed moisture fluxes were 3.2×10^{-8} kg m^{-2} s^{-1} and 4.3×10^{-8} kg m^{-2} s^{-1}, significantly larger than the fluxes measured in this work and by Thomas (1999). These results cannot be attributed to Δp_v because values would have to be 160 Pa and 220 Pa for the two trials, clearly beyond the error bars. Although condensation was observed within the low-temperature chamber in both trials, the authors argued that the moisture fluxes determined from the chamber without condensation were valid and repeatable, as shown by the agreement of the two trials within ~30%. These results at high RH suggest that temperature is the dominant driving potential. The authors compared their measured moisture fluxes with those calculated according to the models of Burch and Thomas (1991) and Krus (1992). Both models predicted moisture would flow in the same direction as measured in the low RH regime but in the direction opposite of that measured in the high RH regime.

The nonisothermal experiments discussed above, in all cases except one (high RH experiment by Dahl et al. 1996), suggest that when the water vapor pressure is nearly constant on both sides of a plywood or OSB specimen, there may be a small moisture flow. It is unclear which gradient (T, φ, p_v, or some combination) drives the observed moisture flux (except in the case noted above) because there may exist a gradient in water vapor pressure hidden by the experimental error. Further experiments with a variety of other boundary conditions are necessary to discriminate between the different driving potentials.

The nonisothermal measurements reported here should be considered only the beginning of a larger program aimed at determining the full functional dependence of moisture flow coefficients of wood-based materials. Considering Figure 1,

beginning with boundary conditions of type 1, the dependence of the isothermal permeability on both relative humidity and temperature will be determined. Further experiments of type 2 over a broader range of T and φ are necessary, and likewise for the other types of nonisothermal boundary conditions.

CONCLUSIONS

This paper describes research aimed at understanding whether moisture transport in the presence of a temperature gradient is important in wood-based materials. As a precursor toward this objective, the isothermal moisture permeance of 11-mm-thick plywood has been measured as a function of relative humidity at room temperature. Comparison with other data from the literature reveals that permeability values for exterior-grade plywood vary by as much as a factor of four or more. Experiments with conditions of nearly constant water vapor pressure in the presence of a thermal gradient show small moisture fluxes from high RH to low RH (from the cold side to the warm side) that might have been caused by water vapor pressure gradients within the experimental error. Measurements with oriented strand board reported in the literature display a similar ambiguity due to experimental error; in most cases it is unclear which potential drives the moisture transport when the water vapor pressure is nearly constant. Future experiments will help to clarify where thermal gradients and varying temperature levels might have a significant effect on moisture flows in real building envelopes.

REFERENCES

ASTM. 2005. *E 96/E 96M–05, Standard Test Methods for Water Vapor Transmission of Materials.* West Conshohocken, PA: ASTM International.

Avramidis, S.; Hatzikiriakos, S. G.; Siau, J. F. 1994. An irreversible thermodynamics model for unsteady-state nonisothermal moisture diffusion in wood. *Wood Science and Technology* 28:349–358.

Bomberg, M. 1989. Testing water vapor transmission: unresolved issues. In: Trechsel, H. R.; Bomberg, M., eds. *Water vapor transmission through building materials*

and systems: mechanisms and measurement. ASTM STP 1039. Philadelphia: American Society for Testing and Materials: 157–167.

Bomberg, M. 2006. On validation of hygric characteristics for heat, air, moisture models. In: Fazio, P.; Ge, H; Rao, J.; Desmarais, G., eds. *Research in building physics and building engineering.* London: Taylor and Francis: 55–62.

Burch, D. M.; Desjarlais, A. O. 1995. Water vapor measurements of low-slope roofing materials. NISTIR 5681. Gaithersburg, MD: National Institute of Standards and Technology.

Burch, D. M; Thomas, W. C. 1991. An analysis of moisture accumulation in a wood frame wall subjected to winter climate. NISTIR 4674. Gaithersburg, MD: National Institute of Standards and Technology.

Burch, D. M.; Thomas, W. C.; Mathena, L. R.; Licitra, B. A.; Ward, D. B. 1989. Transient moisture and heat transfer in multi-layer non-isothermal walls--comparison of predicted and measured results. In: *Thermal performance of the exterior envelopes of buildings IV* conference proceedings. Atlanta: American Society of Heating, Refrigerating and Air-Conditioning Engineers, Inc.: 513-531.

Burch, D. M; Thomas, W. C.; Fanney, A. H. 1992. Water vapor permeability measurements of common building materials. *ASHRAE Transactions* 98(2):486–494. Atlanta: American Society of Heating, Refrigerating and Air-Conditioning Engineers, Inc.

Chang, S. C.; Hutcheon, N. B. 1956. Dependence of water vapour permeability on temperature and humidity. *ASHAE Transactions* 62:437–450 [Paper 1581]. American Society of Heating and Air-Conditioning Engineers.

Claesson, J. 1993. A few remarks on moisture flow potentials. Internal report, International Energy Agency Annex 24, T1-S-93/01.

Claesson, J.; Hagentoft, C.-E.; Wadsö, L. 1994. Masked edge effects when measuring diffusion coefficients with the cup method. *Polymer Engineering & Science* 34(10):821–826.

Dahl, S. D. 1993. Determination of the moisture storage and transport properites [sic] of common building materials. M.S. Thesis. Minneapolis: University of Minnesota.

Dahl, S. D.; Kuehn, T. H.; Ramsey, J. W.; Yang, C.-H. 1996. Moisture storage and non-isothermal transport properties of common building materials. *HVAC&R Research* 2(1):42–58.

Douglas, J. S. 1991. Determination of moisture transport properties for common building materials: methods and measurements. M.S. Thesis. Minneapolis: University of Minnesota.

Douglas, J. S.; Kuehn, T. H.; Ramsey, J. W. 1992. A new moisture permeability measurement method and representative test data. *ASHRAE Transactions* 98(2):513–519. Atlanta: American Society of Heating, Refrigerating and Air-Conditioning Engineers, Inc.

Douglas, J. S.; Kuehn, T. H.; Ramsey, J. W. 1993. An improved moisture permeability measurement method. *Journal of Testing and Evaluation* 21(4):302–308.

Galbraith, G. H.; McLean, R. C. 1990. Interstitial condensation and the vapour permeability of building materials. *Energy and Buildings* 14(3):193–196.

Galbraith, G. H.; McLean, R. C.; Tao, Z.; Kang, N. 1992. The comparability of water vapour permeability measurements: investigation assessing comparability of measured vapour permeability values obtained from range of laboratories throughout European Community. *Building Research and Information* 20(6):364–372.

Galbraith, G. H.; McLean, R. C.; Guo, J. 1997. The selection of appropriate flow potentials for moisture transport models. In: Building simulation conference proceedings, Paper 199. Prague: International Building Performance Simulation Association. 4 p.

Galbraith, G. H.; McLean, R. C.; Gillespie, I.; Guo, J.; Kelly, D. 1998a. Nonisothermal moisture diffusion in porous building materials. *Building Research and Information* 26(6):330–339.

Galbraith, G. H.; McLean, R. C.; Guo, J. S. 1998b. Moisture permeability data presented as a mathematical relationship. *Building Research and Information* 26(3):157–168.

Galbraith, G. H.; Guo, J. S.; McLean, R. C. 2000. The effect of temperature on the moisture permeability of building materials. *Building Research and Information* 28(4):245–259.

Greenspan, L. 1977. Humidity fixed points of binary saturated aqueous solutions. *Journal of Research of the National Bureau of Standards–A. Physics and Chemistry* 81A(1):89–96.

Hansen, K. K.; Bertelsen, N. H. 1989. Results of a water vapor transmission round-robin test using cup methods. In: Trechsel, H. R.; Bomberg, M., eds. *Water vapor transmission through building materials and systems: mechanisms and measurement*. ASTM STP 1039. Philadelphia: American Society for Testing and Materials: 91–100.

Hansen, K. K.; Lund, H. B. 1990. Cup method for determination of water vapour transmission properties of building materials: sources of uncertainty in the method. In: Vincent, T. J., ed. *Building physics in the Nordic countries: proceedings of the 2nd symposium*. Trondheim, Norway: Tapir Publishers: 291–298.

Hens, H. 1996. Final Report, Vol. 1, Task 1: Modelling. International Energy Agency Annex 24—Heat, Air and Moisture Transfer Through New and Retrofitted Insulated Envelope Parts (HAMTIE). Leuven, Belgium: Katholieke Universiteit Leuven, Departement Burgerlijke Bouwkunde, Laboratorium Bouwfysica.

Hoffee, A. R. 1989. Variability of water vapor transmission rates of extruded polystyrene using ASTM E 98–80 (dessicant method). In: Trechsel, H. R.; Bomberg, M.,

eds. *Water vapor transmission through building materials and systems: mechanisms and measurement.* ASTM STP 1039. Philadelphia: American Society for Testing and Materials: 123–133.

Hyland, R. W.; Wexler, A. 1983. Formulations for the thermodynamic properties of the saturated phases of H_2O from 173.15 K to 473.15 K. *ASHRAE Transactions* 89(2A):500–519. Atlanta: American Society of Heating, Refrigerating and Air-Conditioning Engineers, Inc.

Joy, F. A.; Wilson, A. G. 1965. Standardization of the dish method for measuring water vapour transmission. In: *Proceedings of the international symposium on humidity and moisture.* New York: Reinhold Publishing Co.: Vol. 4, 259–270 [Chapter 31].

Karagiozis, A. N. 2001. Advanced numerical models for hygrothermal research. In: Trechsel, H. R., ed., *Moisture analysis and condensation control in building envelopes*, ASTM MNL40. West Conshohocken, PA: American Society for Testing and Materials: 90–106 [Chapter 6].

Krus, M. 1992. Does vapor diffusion really depend on moisture content? Internal report, International Energy Agency Annex 24, T3-D-92/02.

Krus, M. 1994. Non-isothermal moisture movement in wood: an interpretation of the results of Siau et al. Internal report, International Energy Agency Annex 24, T3-D-94/01.

Krus, M. 1996. Moisture transport and storage coefficients of porous mineral building materials: theoretical principles and new test methods. Stuttgart, Germany: Fraunhofer IRB Verlag.

Kumaran, M. K. 1987. Moisture transport through glass-fibre insulation in the presence of a thermal gradient. *Journal of Thermal Insulation* 10:243–255.

Kumaran, M. K. 1988. Comparison of simultaneous heat and moisture transport through glass-fibre and spray-cellulose insulations. *Journal of Thermal Insulation* 12:6–16.

Kumaran, M. K. 1989. Vapor transport characteristics of mineral fiber insulation from heat flow meter measurements. In: Trechsel, H. R.; Bomberg, M., eds. *Water vapor transmission through building materials and systems: mechanisms and measurement.* ASTM STP 1039. Philadelphia: American Society for Testing and Materials: 19–27.

Kumaran, M. K. 1996. Final Report, Vol. 3, Task 3: Material Properties. International Energy Agency Annex 24—Heat, Air and Moisture Transfer Through New and Retrofitted Insulated Envelope Parts (HAMTIE). Leuven, Belgium: Katholieke Universiteit Leuven, Departement Burgerlijke Bouwkunde, Laboratorium Bouwfysica.

Kumaran, M. K. 1998. Interlaboratory comparison of the ASTM standard test methods for water vapor transmission of materials (E 96–95). *Journal of Testing and Evaluation* 26(2):83–88.

Kumaran, M. K. 2002. A thermal and moisture transport property database for common building and insulation materials. Final Report, ASHRAE Research Project RP-1018. Atlanta: American Society of Heating, Refrigerating and Air-Conditioning Engineers, Inc.

Kumaran, M. K.; Lackey, J. C.; Normandin, N.; Tariku, F.; van Reenen, D. 2003. Variations in the hygrothermal properties of several wood-based building products. In: Carmeliet, J.; Hens, H.; Vermeir, G., eds. *Research in building physics.* Lisse, The Netherlands: Swets and Zeitlinger: 35–42.

Künzel, H. M. 1995. Simultaneous heat and moisture transport in building components: one- and two-dimensional calculation using simple parameters. Stuttgart, Germany: Fraunhofer IRB Verlag.

McLean, R. C.; Galbraith, G. H.; Sanders, C. H. 1990. Moisture transmission testing of building materials and the presentation of vapour permeability values. *Building Research and Practice* 18(2):82–91.

Meyer, S. L. 1975. *Data analysis for scientists and engineers.* New York: John Wiley & Sons.

Mukhopadhyaya, P.; Kumaran, M. K.; Lackey, J. 2005. Use of the modified cup method to determine temperature dependency of water vapor transmission properties of building materials. *Journal of Testing and Evaluation* 33(5):316–322.

Osanyintola, O. F.; Talukdar, P.; Simonson, C. J. 2006. Transient moisture transfer between spruce plywood and humid air. In: Fazio, P.; Ge, H; Rao, J.; Desmarais, G., eds. *Research in building physics and building engineering.* London: Taylor and Francis: 11–18.

Peuhkuri, R. 2003. Moisture dynamics in building envelopes. Ph.D. Thesis [Report R-071]. Lyngby: Technical University of Denmark, Department of Civil Engineering.

Schwartz, N. V.; Bomberg, M.; Kumaran, M. K. 1989. Water vapor transmission and moisture accumulation in polyurethane and polyisocyanurate foams. In: Trechsel, H. R.; Bomberg, M., eds. *Water vapor transmission through building materials and systems: mechanisms and measurement.* ASTM STP 1039. Philadelphia: American Society for Testing and Materials: 63–72.

Segerholm, I. 2002. Moisture transport in wood exposed to a temperature gradient: an experimental method. In: Gustavsen, A.; Thue, J. V., eds. *Building physics in the Nordic countries: proceedings of the 6th symposium.* Trondheim, Norway: Norwegian University of Science and Technology: 365–371.

Segerholm, I. 2003. Moisture transport in wood exposed to a temperature gradient—results from experiments. In: Carmeliet, J.; Hens, H.; Vermeir, G., eds. *Research in building physics.* Lisse, The Netherlands: Swets and Zeitlinger: 169–176.

Thomas, W. C. 1999. Moisture transfer in porous materials exposed to combined humidity and temperature gradi-

ents. Final Report, ASHRAE Research Project RP-810. Atlanta: American Society of Heating, Refrigerating and Air-Conditioning Engineers, Inc.

Toas, M. 1989. Results of the 1985 round-robin test series using ASTM E 96–80. In: Trechsel, H. R.; Bomberg, M., eds. *Water vapor transmission through building materials and systems: mechanisms and measurement.* ASTM STP 1039. Philadelphia: American Society for Testing and Materials: 73–90.

Tveit, A. 1966. Measurements of moisture sorption and moisture permeability of porous materials. Report No. 45. Oslo: Norwegian Building Research Institute.

Valovirta, I.; Vinha, J. 2004. Water vapor permeability and thermal conductivity as a function of temperature and relative humidity. In: *Performance of exterior envelopes of whole buildings IX* conference proceedings [CD-ROM]. Atlanta: American Society of Heating, Refrigerating and Air-Conditioning Engineers, Inc.

APPENDIX A: ERROR ANALYSIS

The cumulative uncertainty in permeance, as will be shown below, is given by

$$\varepsilon(M) = (1 + MZ_a)\sqrt{\varepsilon(A)^2 + \varepsilon(p_{sat})^2 + \varepsilon(\Delta\varphi)^2 + \varepsilon(\dot{m})^2 + \varepsilon(c_{edge})^2} + MZ_a\varepsilon(Z_a),$$

(A-1)

where $\varepsilon(x)$ represents the relative error in x. The absolute error in x will be represented by $E(x) = x \cdot \varepsilon(x)$. Permeance is calculated (compare to Equation 6) as

$$M = \frac{1}{Z_{total} - Z_a},$$ (A-2)

where

$$Z_{tot} = \frac{A \cdot p_{sat}(T) \cdot \Delta\varphi}{\dot{m} \cdot c_{edge}} = \text{the total measured resistance,} \quad \text{m}^2 \cdot \text{s} \cdot \text{Pa} \cdot \text{ng}^{-1}.$$

The sources of uncertainty in all of the measured values are discussed below. If the errors in A, p_{sat}, $\Delta\varphi$, $\dot{m}$, and c_{edge} are assumed to be independent and uncorrelated, then the relative error in Z_{tot} can be calculated as (Meyer 1975)

$$\varepsilon(Z_{tot}) = \sqrt{\varepsilon(A)^2 + \varepsilon(p_{sat})^2 + \varepsilon(\Delta\varphi)^2 + \varepsilon(\dot{m})^2 + \varepsilon(c_{edge})^2}.$$

(A-3)

This assumption is not strictly correct, but is probably reasonable. First, $\varepsilon(\dot{m})$ is dependent on $\varepsilon(p_{sat})$ and $\varepsilon(\varphi)$ since the leakage rate is calculated from vapor pressure; however, the uncertainty in vapor pressure is very small compared to the uncertainty in the fit for the leakage rate. Second, $\varepsilon(c_{edge})$ and $\varepsilon(A)$ are correlated since both are geometric and depend on the condition of the waxed edge and the uncertainty in diameter. However, it can be shown that this correlation leads to a smaller error than that given by Equation A-3 since these errors are in the same direction and some cancellation occurs.

For example, if the area used in calculating Z_{tot} is smaller than the actual area, the masked edge correction factor will also be too small, but the error in (A/c_{edge}) should be minimal.

Z_a is determined from several measurements of Z_{tot}, so the errors in these terms are not independent. Equation A-1 was derived by adding the absolute errors in Z_{tot} and Z_a: $E(M) = E(Z_{tot}) + E(Z_a)$.

Area of the Specimen, *A*

The uncertainty in the exposed surface area A arises from (i) the tolerance in the diameter of the hole in the test ring, ±0.25 mm; (ii) misalignment of the template over the hole in the test ring; and (iii) an imperfectly formed wax seal where the template meets the specimen. The cumulative error in diameter from all three sources is estimated at 1.5 mm, yielding a relative uncertainty in A of 1% for specimens with an exposed diameter of 305 mm (note that $\varepsilon[A] = 2\varepsilon[d]$).

Water Vapor Saturation Pressure, $p_{sat}(T)$

Uncertainties in $p_{sat}(T)$ arise from (i) repeatability of the temperature sensors, (ii) fluctuations in temperature at steady state, (iii) non-uniformity of the chamber environments, and (iv) the mathematical expression for $p_{sat}(T)$. The uncertainty in the measured temperature is ±0.1 K. Temperature fluctuations at steady state are generally within ±0.05 K. Because the chamber air is mixed by fans, thermal gradients within the chamber should be minimal. $p_{sat}(T)$ is calculated from the expression of Hyland and Wexler (1983). The error in the mathematical expression, estimated at less than 0.03%, is negligible. The combined uncertainty of ±0.15 K yields a relative uncertainty in the saturation vapor pressure of 0.9%.

Relative Humidity Difference, $\Delta\varphi$

The sources of uncertainty in relative humidity are similar to those for temperature. Uncertainty in the sensor measurements is ±0.01 for $\varphi < 0.90$ and ±0.02 for $\varphi \geq 0.90$. Fluctuations are negligible in comparison to the measurement uncertainty. Mixing of air by fans should minimize stratification. The relative error in $\Delta\varphi$ thus depends on the absolute errors in φ_A and φ_B and the magnitude of the difference between φ_A and φ_B.

$$\varepsilon(\Delta\varphi) = \frac{\sqrt{E(\varphi_A)^2 + E(\varphi_B)^2}}{\varphi_A - \varphi_B}$$ (A-4)

Mass Transfer Rate, $\dot{m}$

Random errors arise from (i) repeatability of the balances, (ii) fluctuations due to airflow dynamics, and (iii) error in the time interval between measurements. Possible systematic errors include (iv) drift due to the balances not being level or being affected by the temperature and humidity conditions in the chamber and (v) mass transfer between the chambers and the laboratory.

Balances are calibrated with a certified calibration standard. Fluctuations are minimized by covering the balance pan and dish containing the salt solution with a draft shield which has a 5-cm-diam opening. Time uncertainty in the computer-based data acquisition system is negligible. Drift is estimated by weighing a calibration standard before and after each experiment. The uncertainty due to drift is less than 0.1%. The balance repeatability error (±2 mg) is minimized by acquiring data for a sufficient time such that the total weight change at steady state conditions is at least 500 mg, yielding a relative uncertainty of 0.4%. This results in a relative uncertainty in the total measured water vapor transmission rate $\dot{m}_{tot}$ of 0.5%.

Water vapor transfer between the chambers and the laboratory ($\dot{m}_{leak}$) is determined from a series of experiments. The environment in the laboratory is maintained at $23 \pm 1°C$ and $50 \pm 2\%$ RH. The two chambers are joined with an impermeable material (acrylic plastic) between them, and the relative humidity in each chamber is controlled with a desiccant or saturated salt solution. The mass transfer rate at steady state is plotted as a function of the water vapor pressure in the chamber, as shown in Figure A-1. A linear least-squares regression analysis based on six measurements gives $\dot{m}_{leak}$ as a function of p_v:

$$\dot{m}_{leak}/ng \cdot s^{-1} = -0.877 \cdot p_v/Pa + 1180 \qquad (A-5)$$

The uncertainty in $\dot{m}_{leak}$ from the fit is 200 ng·s^{-1} (one standard deviation of the residuals). The relative uncertainty in $\dot{m} = \dot{m}_{total} - \dot{m}_{leak}$ is then calculated from

$$\varepsilon(\dot{m}) = \frac{1}{\dot{m}}[E(\dot{m}_{total}) + E(\dot{m}_{leak})] , \qquad (A-6)$$

where $E(\dot{m}_{tot}) = 0.005 \cdot \dot{m}_{total}$ and $E(\dot{m}_{leak}) = 200$ ng·s^{-1}.

The value of $\dot{m}$ is calculated as the average of $\dot{m}_A$ and $\dot{m}_B$. If these differ by more than the uncertainty in $\dot{m}$ calculated from Equation A-6, then $\varepsilon(\dot{m})$ is taken as

$$\varepsilon(\dot{m}) = \frac{\dot{m}_A - \dot{m}_B}{\dot{m}_A + \dot{m}_B} . \qquad (A-7)$$

Masked Edge Correction Factor, c_{edge}

The measured permeance must be corrected for diffusion within the edge masked by the wax seal. The correction factor is calculated from the expression of Claesson et al. (1994),

$$c_{edge} = \frac{1}{1 + \dfrac{2H}{\pi\kappa R} \cdot \ln\left[\dfrac{2}{1 + \exp(-2\pi\kappa B/H)}\right]} , \qquad (A-8)$$

where

H = thickness of the specimen (11 mm),

R = radius of the exposed portion (152 mm),

B = width of the masked edge (3.2 mm),

κ = 1 for diffusion coefficients the same in all directions, and
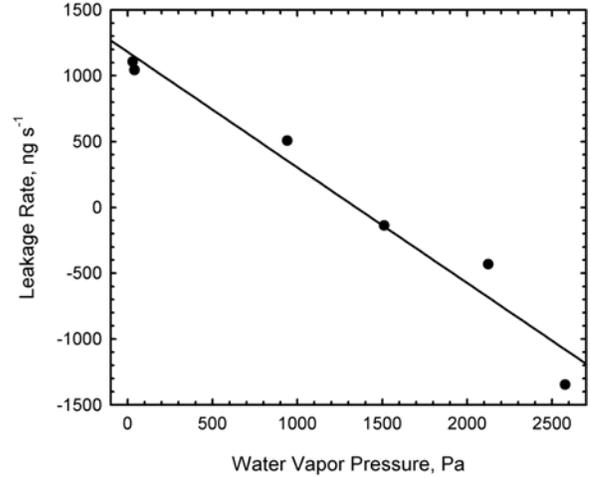
Figure A-1 *Moisture leakage rate into the chamber as a function of the chamber water vapor pressure, along with regression line given by Equation A-5.*

$$\kappa = \sqrt{\frac{2D_z}{D_x + D_y}} \qquad (A-9)$$

for diffusion coefficient D_z perpendicular to the specimen and two different diffusion coefficients D_x and D_y in the plane of the specimen.

The estimated relative uncertainties in the dimensions H, R, and B are 1%, 0.5%, and 10%, respectively. According to Siau (1995) the ratio of the diffusion coefficient for wood in the longitudinal direction to that in the transverse directions can vary from ~100 at low moisture content to ~2 near fiber saturation. If diffusion in the radial and tangential directions is assumed to be the same, then the parameter may vary between ~0.1 and ~1. In order to estimate the uncertainty in c_{edge}, two extreme cases are considered. First, diffusion within the masked edge will be maximized (c_{edge} will be minimized) when H and B are large and R and κ are small. The value obtained with H increased from the measured value by 1%, B increased by 10%, R decreased by 0.5%, and $\kappa = 0.1$ is $c_{edge} = 0.958$. The other extreme occurs when H is decreased by 1%, B decreased by 10%, R increased by 0.5%, and $\kappa = 1$, which yields $c_{edge} = 0.976$. The mean of these two extreme cases is selected with the associated error: $c_{edge} = 0.967 \pm 0.009$. The relative error then is 0.9%.

Surface Air Layer Resistance, Z_a

Douglas et al. (1992) measured the surface air film resistance using the method of Burch et al. (1989). The total resistances were measured with one, two, and three identical layers of gypsum board; these resistances were then plotted versus the number of layers. A linear regression analysis determined the y-intercept (equivalent to the surface film resistance) of 3.3×10^{-4} m^2·s·Pa·ng^{-1}. No uncertainty was reported, and a

10% error is assumed in our calculations. The contribution of the air film resistance to the total uncertainty becomes more significant as the overall permeance M increases, in accord with Equation A-1.

APPENDIX B: CALCULATIONS

In all calculations, it is assumed that the moisture permeance does not depend strongly on temperature for this range (mainly 20–27°C), such that the value at room temperature can be used. The permeance is calculated for the appropriate RH boundary conditions based on the available information in each paper. The water vapor pressure difference Δp_v necessary to induce the observed moisture flux is calculated as

$$\Delta p_v = \frac{J_m}{M}. \qquad (B\text{-}1)$$

This Work

Permeabilities are calculated from the fit to the data shown in Figure 3 and converted to permeance by dividing by the thickness of the specimen (0.011 m).

Experiment I: $J_m = 8000$ ng·m^{-2}·s^{-1}; $M = 210$ ng m^{-2} s^{-1} Pa^{-1}; $\Delta p_v = 38$ Pa.

Experiment II: $J_m = 4400$ ng·m^{-2}·s^{-1}; $M = 160$ ng m^{-2} s^{-1} Pa^{-1}; $\Delta p_v = 28$ Pa.

Experiment III: $J_m = 800$ ng·m^{-2}·s^{-1}; $M = 160$ ng m^{-2} s^{-1} Pa^{-1}; $\Delta p_v = 5$ Pa.

Thomas 1999

The reported uncertainties in temperature and RH were ±0.2°C and ±0.6%, respectively, which lead to an uncertainty in Δp_v of about 50 Pa for the experimental conditions. The permeance of the 6.4-mm OSB in the 25–45% RH range is taken to be 85 ng m^{-2} s^{-1} Pa^{-1}, the average of seven measurements at RH values below 50%. Three experiments with nearly constant p_v were reported.

"Equal Vapor Pressure": $J_m = 5500$ ng·m^{-2}·s^{-1}; $\Delta p_v = 65$ Pa.

"Test No. 11": $J_m = 4800$ ng·m^{-2}·s^{-1}; $\Delta p_v = 56$ Pa.

"Test No. 12": $J_m = 3300$ ng·m^{-2}·s^{-1}; $\Delta p_v = 39$ Pa.
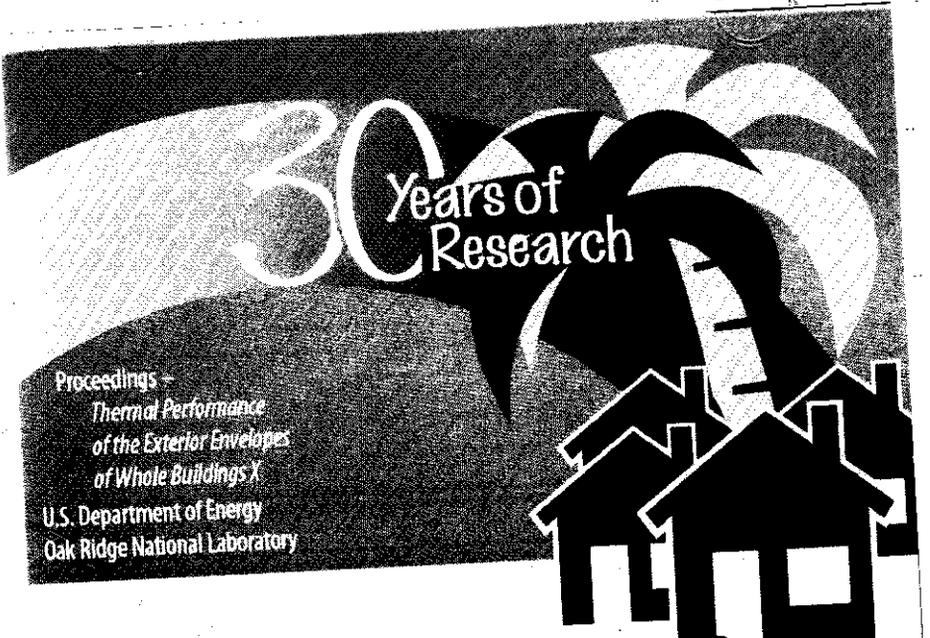
Dahl et al. 1996

The uncertainty in p_v is estimated at 2.2% (see Douglas et al. 1992, 1993), which leads to an error in Δp_v of about 30 Pa for the low RH regime ("OSB 3") and about 60 Pa for the high RH regime ("OSB 6" and "OSB 6R"). The permeance values are the means calculated from measurements reported by the authors for low RH (100 ng·m^{-2}·s^{-1}·Pa^{-1}, two measurements) and high RH (200 ng·m^{-2}·s^{-1}·Pa^{-1}, three measurements).

"OSB 3": $J_m = 12{,}200$ ng m^{-2} s^{-1}; $M = 100$ ng m^{-2} s^{-1} Pa^{-1}; $\Delta p_v = 120$ Pa.

"OSB 6": $J_m = 32{,}000$ ng m^{-2} s^{-1}; $M = 200$ ng m^{-2} s^{-1} Pa^{-1}; $\Delta p_v = 160$ Pa.

"OSB 6R": $J_m = 43{,}400$ ng m^{-2} s^{-1}; $M = 200$ ng m^{-2} s^{-1} Pa^{-1}; $\Delta p_v = 220$ Pa.

30 Years of Research

Proceedings –
*Thermal Performance
of the Exterior Envelopes
of Whole Buildings X*
U.S. Department of Energy
Oak Ridge National Laboratory

Buildings X
CONFERENCE

DEC. 2-7, 2007

ORNL 07-G01409/aas